29th Symposium on Naval Hydrodynamics
Gothenburg, Sweden, 26-31 August 2012

Investigation of Asymmetrical Shaft Power Increase during Ship Maneuvers by means of Model Tests and CFD

S. Mauro, G. Dubbioso, R. Broglia, R. Muscari
(INSEAN-CNR, National Research Council, Maritime Research Centre, Italy)

ABSTRACT

Propulsion systems experience large power absorption fluctuations during tight maneuvers. In the case of a turning circle maneuver for a twin-screw ship, the power required by the two shaft lines can be completely different; in case of non conventional propulsion system, like cross-connect configurations, a compromise must be met in order to design a safe control system, without dramatically affect the vessel's maneuvering performance. In order to investigate the influence of different propulsion system operation settings on the vessel's maneuvering characteristics, a series of had-hoc free running model tests have been carried out at the CNR-INSEAN outdoor maneuvering basin. In the present work experimental results will be presented and discussed, focusing on the ship maneuvering performance under different propulsion system control settings. Moreover, CFD have been used to provide a deeper insight on the propellers overloading and unbalancing: first, numerical computations have been carried out to capture the nominal wake in correspondence of the propeller disks; then, propeller loads were evaluated (off-line the RANSE simulation) by means of two simplified model based on Blade Element Momentum theory (BEMT) theory.

INTRODUCTION

Marine propulsion plants can experience large power fluctuations during tight manoeuvres. During these critical situations, dramatic increase of shaft thrust and torque is possible; in some situation the increase can be up to and over 100% of the steady values in straight course. In case of a twin-screw ship turning circle, the dynamic of the two shaft lines can be completely different, in terms of the required power and torque. A preliminary work [35] was performed in last years analyzing turning circle maneuvers at different speeds and rudder angles performed during sea trials for a series of twin screw naval ships. Results of this analysis allowed to underline a common trend for asymmetrical shaft power increase, despite the wide series of (even rather different) ships considered (Figure 1). In [16] propeller behaviour during turning circle manoeuvre has been investigated by means of LDV measurements carried out on a three propeller naval vessel, with emphasis on propeller cavitation performances.

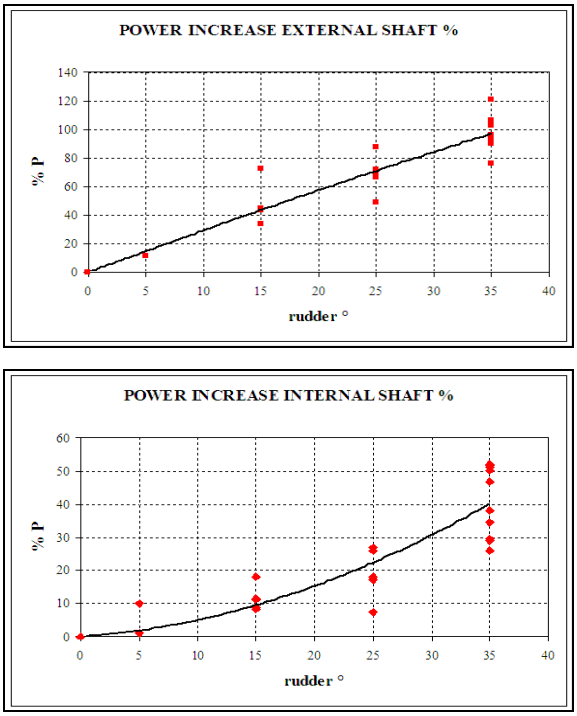

Figure 1: Power increase on the internal and external shaft during turning circle maneuver

Qualitatively, a similar behaviour for the both the external and the internal shaft as depicted in Figure 1 was detected. On the basis of such measurements, the external propeller experiences strong lateral components, whereas, the flow on the internal one is essentially affected by the ship wake and, as a consequence, a flow straightening effect. Atvanapranee [1] investigated the flow field features of a turning naval ship model (DDG51) during a stabilized turn (circular motion test); propeller unbalancing was opposite with respect to the previous observation. This is probably due to the opposite propeller revolution rate (outward from the top when viewing from the stern). It is evident, therefore, that propeller overloading and unbalancing is an extremely complicated phenomenon, strictly related to the ship's wake feature and propeller direction of rotation. As a consequence, this aspect is difficult to predict in a preliminary design phase by

means of simplified approaches, therefore, experimental campaign or detailed numerical simulations represent the only means for a quantitative analysis. On the basis of the outcomes of this studies, it is clear that this phenomenon, if not correctly considered, could be potentially dangerous, especially for propulsion plants with two shaft lines powered via a unique reduction gear (Figure 2), which can be subject to significant unbalances.

This kind of propulsion plant, despite not very common, has been recently proposed as a solution for particular applications, such as fast naval ships (patrol vessels, frigates). In these cases, automation plant needs to monitor carefully these effects, in order to avoid any possible problems. Moreover, large asymmetrical shaft power during maneuver might result in different dynamical behavior of the ship, with effects on both the transient and the stabilized phases. Another aspect that can have important effects on the turning ability characteristics of the vessel, is the strategy adopted by the automation plant (i.e. constant RPM, constant power or constant torque strategy). In this work a series of novel free running model tests designed at the INSEAN-CNR outdoor maneuvering basin (sited at the Nemi Lake) will be presented. In particular, the main focus is to reproduce at model scale the different propulsion power plant configurations, which is of cross connect type, as shown in Figure 2.

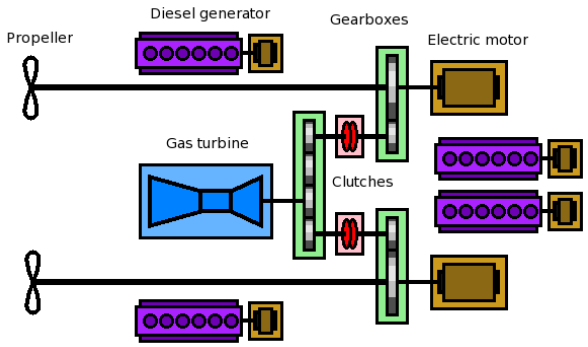

Figure 2: Cross connect propulsion system configuration.

Moreover, it is evident that the reduction gear is a critical component of this plant, because at certain configurations (namely maximum speed operations) it drives both shafts; during tight maneuvers, it can be stressed excessively by fluctuating loads due to the large differences in power demanding between internal and external shafts. Therefore, in order to quantify the maximum loads experienced, it is mandatory to characterize the propulsion system behavior in a wide range of operational conditions. These information are crucial for a correct sizing of the propulsion system and the design of the automation control system, which must prevent both prime mover and shafting be working in dangerous regimes. On the other hand, the effects of different automation control system settings on the vessel maneuvering behavior should be investigated in order to provide useful guidelines for the control system's logic development. To this purpose, in the tests presented in this paper, in addition to the usual maneuver macroscopic parameters (advance, transfer, tactical diameter, turning diameter and speed), both thrust and torque experienced by both propeller shafts have been measured; this allowed a complete characterization of the propulsion system behavior.

To these aims, turning circle (with and without pull-out) and Zig-Zag maneuvers at different rudder angles and speeds (*Fn=0.26* and *Fn=0.367*) have been carried out; this allowed to cover a broad spectrum of dynamic conditions (i.e. speed and drift angle). Moreover, different propulsion system strategies have been tested: constant propeller revolution rate (which is the standard procedure usually followed in this kind of tests) and prime movers constant torque and power . This is of paramount importance since it allows to model all the possible propulsion system strategies at full scale.

In order to investigate and gain more insight into the phenomenon, features of the stern flow field during the stabilized phase of the turning have been numerically predicted by means of the unsteady Reynolds averaged Navier-Stokes Equations (uRaNSE) solver *χnavis* developed at CNR-INSEAN. In particular, the simulations have been carried out at the same kinematics conditions experienced during the test (same yaw rate, absolute speed and drift, neglecting roll angle) in order to evaluate the velocity field (i.e. the nominal wake) in correspondence of the propellers planes. In these preliminary computations, a simplified geometry has been investigated; namely, the bare hull fitted with bilge keels and centerline skeg without propeller shafts and brackets. The choice for this simplified configuration is supported by the numerical results of a maneuvering ship presented in [3][11], where it was emphasized that the strong vortical structures developed during the maneuver were primarily originated in correspondence of the bilge keels and the skeg.

Propeller loads (thrust and torque) corresponding to the computed nominal wake (on both the internal and external side) are evaluated off-line from the uRaNSE solver. Propellers are modeled by means of a suitable Blade Element and Momentum Theory (BEMT) model extended to treat oblique flow [19]; in this model, the propeller blades are described by means of the hydrodynamic characteristics of 2D sections encountering a variable flow in terms of angle of attack and flow magnitude during one complete revolution. In particular, in order to investigate the effect of unsteadiness met by a propeller section during a

complete revolution, an unsteady BEMT model based on indicial theory [17][25][26] has been also considered. The principal aim of present investigation is to check the capabilities of simplified models to correctly represent the presence of a propeller. It has to be observed that BEM or fully RANSE approaches, which take into account for the complete three dimensional geometry of the propeller, would lead to a better representation of the complex interaction between propeller and hull and loads developed, but at the expense of computational resource and CPU time. On the other hand, the BEMT models, despite their simplicity, can be considered as a valid alternative to sophisticated models, if the detailed flow features arising from the complex hull-propeller interactions are of second relevance, as in this context where the main focus is on the prediction of propeller loads, providing a reliable description of the propeller during off design conditions, like a turning maneuver may be considered. Moreover, the comparison of computed thrust and torque with respect to the experiments allow a valuable guidance for further developments and improvements of propeller models, when dealing with propeller in off-design conditions. As a final remark, the experimental activity presented in this work will provide a complementary test case on the propeller asymmetrical behavior with respect to the experimental (and numerical) activity described in [1][16], where an analogous naval vessel, but different stern form geometry has been investigated.

Latest, the present analysis can be useful for the improvement of had-hoc modules into full mission maneuvering mathematical models; namely, those one that aim to model both ship and propulsion system dynamics, as the one presented in [9][27][34], for a more accurate treatment of propeller overloading and unbalancing.

Table 1: Model geometric characteristics

L/B	*7.531*
B/T	*3.286*
C_B	*0.51*
A_R/LT	*3.2%*
D_{PROP}	*0.29*
N_{BLADES}	*5*
P/D	*1.3*
A_{EXP}	*0.78*

EXPERIMENTAL SETUP

The ship selected for the present analysis is a twin screw naval ship, i.e. a similar configuration to those analyzed in previous studies [9][35]. In Table 1, main ship and propeller characteristics are reported: L is ship length, B is ship beam, T is draft, CB is block coefficient and A_R is total longitudinal projected rudder area. Propellers rotate inward from the top viewing from astern. The measurements equipment installed on the model are schematized in Figure 3. The experimental activities are carried out at the Nemi natural volcanic lake located 40 km far from the main CNR-INSEAN branch.

It is an ideal location where long-term dead-calm water conditions are frequent in a non-anthropic natural and environmentally protected area. The water surface is large enough to allow the execution on any kind of maneuvering test regardless the model size and speed. For the sake of clarity, the following Figure 4 with a Google map® satellite view (Decimal GPS coordinate lat.12.700377702713013 long. 41.720448924843765) and the official ITTC facility data sheet are included.

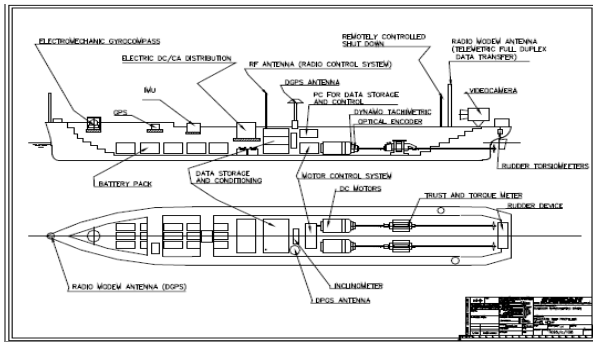

Figure 3: Model setup

On-board the unmanned model, each propeller shaft is driven by a dedicated brushless motor; the whole instruments energy demand is provided by a diesel electric generator. Each shaft line is equipped by a dynamometer for the measurements of propeller loads, namely torque and thrust; in particular, the measurement of thrust demand is a novel element with respect to the experiments presented in [35] at full and model scale. Moreover, in order to reproduce the cross-connect propulsive configuration (full scale, highest speed) both shafts are linked by means of a chain and a suitable reduction gear; this guarantees the cross-connect configuration adopted at the highest speed to be properly simulated. The self-propelled unmanned free-running model is fully equipped with all the technical devices necessary to carry out the experimental activities: DGPS, IMUs, torque and thrusts meters on the propeller axis, dynamo-tachometers, real-time data transmission devices, etc.

CONTROL SYSTEM DESIGN

Propulsion system control is of central importance during tight maneuvers, in particular at high speed, since loads experienced by the shaft line devices (reduction gear, bearings) increase dramatically.

INTERNATIONAL TOWING TANK CONFERENCE CATALOGUE OF FACILITIES
TOWING TANKS, SEAKEEPING AND MANOEUVRING BASINS

ISTITUTO NAZIONALE PER STUDI ED ESPERIENZE DI ARCHITETTURA NAVALE (INSEAN)
Via di Vallerano 139, I-00128 Roma, ITALY
TEL +39-06-50299-1; FAX +39-06-5070619
Web URL: "http://www.insean.it"

ITALY

MANOEUVRING BASIN (Situated on Nemi natural lake – 1953)

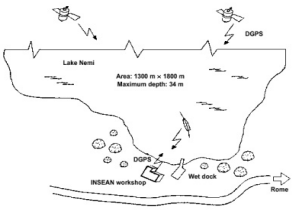

Description: outdoor natural basin, test area = 1300 m × 1800 m, maximum depth = 34 m

Instrumentation: gyro for measuring course angle and its rate of change; balance dynamometer for measuring forces and torque acting on the rudder; model propeller torque and thrust transmission dynamometers; DC tachometer for propeller revolution; rudder angle potentiometer, ship position by DGPS, log, computerised data collection and processing system; model motor power supplies up to 4 kW

Model size range: 1.5m ÷ 8.0 m

Model tracking techniques: radio controlled by operator during shore approaching and leaving or in emergency case; computer controlled during manoeuvring tests

Tests performed: standard manoeuvring tests, such as: (1) zig-zag, (2) turning circle, (3) weave, (4) pull out, (5) spiral test, (6) crash stop, etc.

Published description: INSEAN web site, January 2002

Figure 4*:* Outdoor CNR-INSEAN ship maneuvering model basin

As described above, this topic is further stressed in case of shaft lines connected via a unique reduction gear: this element is the critical one because, due to the different torque required by the propellers, it experiences relevant pulsating loads during each revolution. In order to investigate the propulsion system working regime on the maneuvering capabilities, a control system device has been developed. The control tool is demanded to limit the power/torque provided by the two electric motor to the propeller shaft at a prescribed value. In the present analysis, the total loads on the two shaft during the approach phase (i.e., the straight path phase before the rudder action) is assumed as a reference and the control system allows only a percentage increase above it; in the experimental results that will be presented, both power and torque are limited to the value experienced in the approach phase. In particular, the control system acts to limit the feeding voltage to the brushless motor in order to fix the power/torque release. To this aim, the coupling between the limit voltage V_{LIM} and power/torque release has been approximately determined by means of suited tests. In particular, turning test are carried out at the desired speed; after the rudder is actuated, V_{LIM} is reduced by small fractions and kept constant until the model reaches a new stabilized phase and the corresponding total loads are collected. For the sake of clarity, in Figure 5 is reported such kind of repeated turning tests: it can be observed that as V_{LIM} (light blue curve) is decreased, propeller revolution (dark blue curve) decreases because the power/torque (red curve) furnished by the mover is lower with respect the required one.

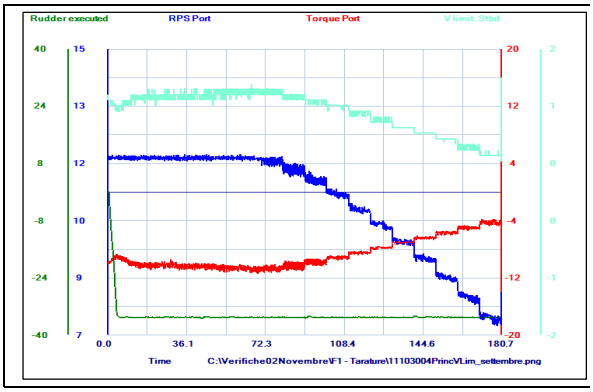

Figure 5: Voltage Limit Control for PORT shaft

During the maneuvering test, the control system monitors the torque/power at each instant; when the propeller power/torque demanding overcomes the prescribed one, the V_{LIM} is gradually changed to the value obtained from previous tests.

EXPERIMENTAL RESULTS

Standard maneuvering tests, namely turning circle with pull out, Zig-Zag and Dieudonnè spiral maneuver have been carried out with three different propulsion strategies: constant RPM, constant torque and constant power. In the controlled maneuvers, torque and power have been fixed to the value in the approach phase. In the following discussion, only turning circle results will be deeply considered, since they are the most suitable for gaining more insight into the key aspects of the propeller overloading and unbalancing phenomena. Moreover, it has to be pointed out that this phenomenon is more evidenced at the highest rudder angle (i.e. 35°), being the flow field markedly changed from the straight motion one because of the largest lateral velocity in the horizontal plane.

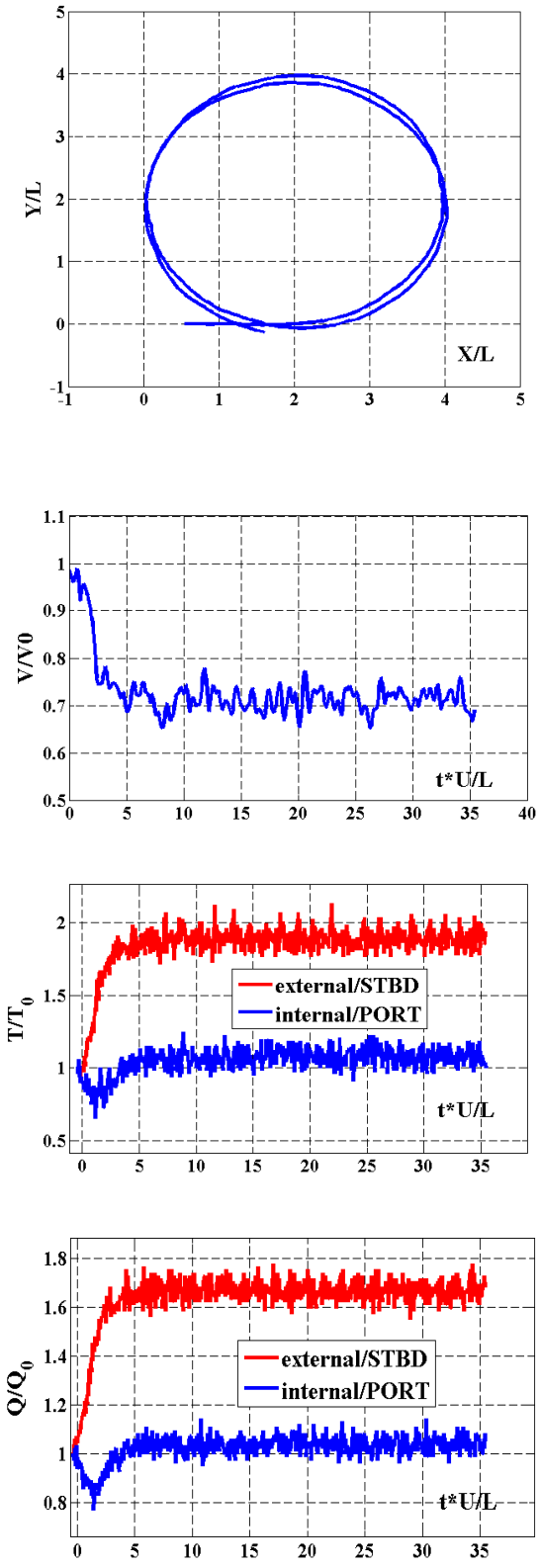

Figure 6: Turning Circle (constant RPM) measurement outcomes

As it has already shown in [3][11], due to this strong cross flow, intense vortical structures and separation regions are generated and convected astern asymmetrically with respect to the hull symmetry plane, causing the appearance of asymmetric wake in correspondence of the internal and external propellers.

The outcomes of the measurement devices relative to vessel's kinematics and propulsion system behavior are reported in Figure 6 in case of the constant RPM maneuver at the maximum rudder angle (35°) at F_N=0.26: trajectory, speed drop and thrust and torque on both the internal and the external shaft are shown; propeller loads are normalized with the straight approach phase T_0 and Q_0. It can be evidenced that, after the rudder is actuated, thrust and torque experience a marked increase differently on both shafts: in particular, on the external shaft thrust and torque increase by 80% and 60% with respect the value in the approach phase, respectively; whereas, propeller on the internal side is lightly overloaded (thrust 20%, torque 10%). At the highest speed (F_N=0.37) internal shaft does not experience an increase in torque/thrust demanding, whereas, the external one experiences an increase in torque (40% and thrust 70%). This behavior qualitatively confirms the trends reported in Figure 1 for the torque absorption; asymmetrical loads demanding are strictly related to the asymmetric wake developed during the combined sway-yaw motion of the vessel in a turn. It has to be pointed out that, at full scale and at the highest speed, the two shaft lines are connected via the unique reduction gear; it is evident that discrepancies among the internal and the external shaft are critical for this component and the action of the automation control system is demanded in order to alleviate the magnitude of pulsating loads.

In Table 2 macroscopic parameters of the turning circle manoeuver are summarized; advance (ADV), transfer (TR), tactical diameter (TD), turning radius (FD) and speed drop relative to the rudder angles are investigated. In Table 3 percentage increase of thrust and torque with respect to the values in the approach phase are summarized. It is worth noting that the propeller unbalancing and overloading is emphasized during the tightest maneuvers. In order to verify the measurements, a repeatability analysis has been performed; in particular, in Table 2 and Table 3, mean value and r.m.s. (in brackets) of turning maneuvering parameters and percentage increase of thrust and torque for the 35° STBD and PORT maneuvers are reported. Repeatability analysis is carried out on the basis of 10 tests for each rudder angle. It can be observed that measurements can be considered reliable, especially if it is taken into account that tests have been carried out in an outdoor basin; discrepancies on the macroscopic parameters are below 2%, whereas propeller loads uncertainty is below 5%. Moreover, good repeatability properties are confirmed observing their symmetrical behavior relative to starboard and port side rudder angles.

Table 2: Turning Circle maneuver results F_N=0.267 (r.m.s. in brackets)

	-35	-25	-15	15	25	35
ADV	3.72 (0.17)	3.87	5.46	5.55	3.99	3.72 (0.21)
TRA	1.73 (0.13)	1.99	3.53	3.63	2.03	1.71 (0.11)
DT	4.22 (0.26)	4.85	8.15	8.3	4.94	4.38 (0.18)
FD	4.36 (0.25)	4.99	8.02	8.15	5	4.41 (0.18)
U/U0	0.73 (0.017)	0.84	0.91	0.92	0.77	0.78 (0.035)

For the sake of completeness, in Table 4 and Table 6 maneuvering and propulsion data relative to the highest speed are summarized:

Table 3: Propeller overloading (r.m.s. in brackets)

	-35	-25	-15	15	25	35
K_T INT	14.83 (2.57)	2.3	5.44	3.2	4.32	14 (2.57)
K_T EST	78.81 (8.91)	61.19	26.47	26.15	64.04	84 (8.9)
K_Q INT	8.6 (1.95)	0.98	1.78	2.08	2.77	17.98 (1.95)
K_Q EST	63 (4.98)	49.24	21.73	25.12	46.36	60 (6.21)

Table 4: Turning Circle maneuver results F_N=0.36 (r.m.s. in brackets)

	-35	-25	-15	15	25	35
ADV	4.22 (0.09)	4.67	6.28	5.90	4.71	4.22 (0.045)
TRA	2.00 (0.1)	2.33	4.55	3.83	2.63	1.94 (0.15)
DT	4.69 (0.11)	5.53	9.17	8.56	5.69	4.84 (0.145)
FD	4.68 (0.12)	5.45	8.95	8.64	5.57	4.80 (0.1)
U/U0	0.81 (0.02)	0.88	0.96	0.96	0.88	0.82 (0.01)

In Figure 7 propulsion system behavior at constant torque and power settings, and for the lowest speed, is reported; in particular ratios of shaft revolutions, torque and thrust with respect to the values in the approach phase are compared to the constant RPM configuration. For the sake of brevity only the external propeller is reported, the following discussion is also valid for the internal one.

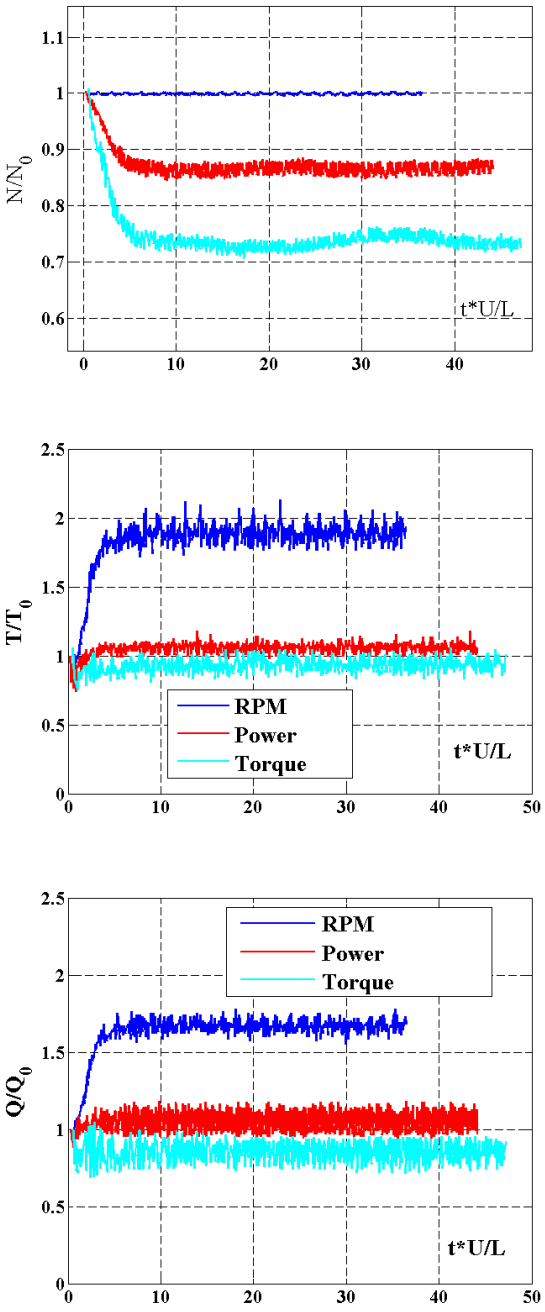

Figure 7: RPM, thrust and torque ratio for different propulsion strategies

It can be evidenced that, after the maneuver is started, the control device acts in order to maintain torque/power to the same value recorded in the approach phase. The measured turning circle parameters at the lowest speed for the constant power and torque tests are summarized in Table 6 and Table 7, respectively; as it will be discussed in the next paragraph, the effect of control system on the maneuvering behavior is negligible.

Table 5: Propeller overloading (r.m.s. in brackets) – constant RPM

	-35	**-25**	**-15**	**15**	**25**	**35**
K_T INT	6.7 (1.82)	0	0.5	0.35	1.25	6.06 (0.8)
K_T EST	57.2 (9.9)	42	19.7	17.3	46	66.48 (0.82)
K_Q INT	3.11 (1.42)	-0.5	0.2	0.5	1.5	3.52 (1.08)
K_Q EST	55.2 (2.19)	36	18.54	14.8	37	52 (0.68)

Table 6: Trajectory parameters (r.m.s. in brackets) - constant TORQUE

	-35	**-25**	**-15**	**15**	**25**	**35**
ADV	3.53 (0.27)	3.87	5.27	5.49	3.94	3.72 (0.089)
TRA	1.7 (0.12)	2.07	3.66	3.37	1.99	1.67 (0.23)
DT	4.24 (0.164)	4.96	8.22	7.75	4.99	4.26 (0.23)
FD	4.38 (0.19)	5.07	8.23	7.71	4.82	3.99 (0.33)
U/U0	0.65 (0.075)	0.73	0.89	0.84	0.68	0.56 (0.092)

Table 7: Trajectory parameters (r.m.s. in brackets) - constant POWER

	-35	**-25**	**-15**	**15**	**25**	**35**
ADV	3.63 (0.13)	3,81	5.92	5.06	3.57	3.28 (0.085)
TRA	1.66 (0.056)	2.06	3.69	3.42	1.96	1.75 (0.043)
DT	4.27 (0.034)	4.91	8.42	7.93	4.72	4.13 (0.045)
FD	4.18 (0.063)	5.11	8.18	8	4.92	4.23 (0.05)
U/U0	0.66 (0.013)	0.81	0.94	0.88	0.78	0.69 (0.013)

Similar results at the highest speed have been observed (not reported for the sake of brevity).

PROPULSION SYSTEM CONFIGURATION: INFLUENCE ON MANOEUVRING CAPABILITIES

In Table 8 trajectory (advance, transfer, tactical diameter and final diameter) and kinematic parameters (speed drop) for the turning circle tests at both F_N and at the maximum rudder angle for the different propulsion strategies considered are summarized. It can be observed that, moving from constant propeller revolution to anyone of the controlled settings does not influences considerably the vessel dynamic response; it has to be noticed that speed reduction is more evident in case of constant torque/power configuration. This is due to the reduction in the propeller thrust caused by the control action, which reduces the maximum delivered prime movers power (and, as a consequence, shaft RPM).

Table 8: Turning parameters at different propulsion settings

FN=0.26	**ADV**	**TRA**	**DT**	**FD**	**U/U_0**
RPM	3.72	1.72	4.30	4.39	0.76
TORQUE	3.62	1.69	4.25	4.19	0.60
POWER	3.45	1.70	4.20	4.21	0.68
FN=0.38	**ADV**	**TRA**	**DT**	**FD**	**U/U0**
RPM	4.28	2.07	4.82	4.79	0.82
TORQUE	4.15	1.93	4.56	4.37	0.65
POWER	4.01	1.93	4.50	4.49	0.70

NUMERICAL INVESTIGATION

In the last decades CFD has been extensively verified and validated for typical vessel design issues, namely resistance and self propulsion performance prediction, as demonstrated in International CFD Workshops (Tokyo 2005, Goteborg 2010). On the other hand, aiming to developing reliable numerical tools for broader aspects of ship hydrodynamics, verification and validation of such techniques applied to vessel operating in off-design condition is demanded. The framework of ship maneuverability and related topics, like propulsion device performance, can be considered a valid field for further stressing CFD capabilities and promoting new and efficient solutions to this ambitious task. The presence of the rotating propeller is usually accounted for by means of simplified models, namely those based on the actuator disk theories, like Hough and Hordway or Nakatake's one. The suitability of this approach has been extensively proved in case of ship propulsion performance prediction, i.e. for a design conditions in a straight path. However, present approach in case of off-design conditions like a tight turning maneuver, can provide misleading results because of the leaks in treating oblique flow effects. On the other hand, simplified models based on blade section theory, seems to be a suitable and affordable alternative to the previous one because of their strict relation to the physic involved in propeller flow and their straightforward extension to include oblique flow effects. It is evident that more accurate propeller models, like Boundary Element Method (BEM) or RANSE, would certainly provide a more accurate prediction of the loads generated on the propeller, but at the cost of increased computational resource and time demanding. Reliability of BEMT propeller

modeling in a CFD solver is provided for the study of self propulsion performance of an unmanned underwater vehicle [21]; the same approach has been validated for the prediction of hydrodynamic forces and moments acting on a surface displacement vessel (KVLCC2) performing captive oscillatory motions [19] Typical aspects of propeller performance during oblique flow operations, mainly the nature of propeller in-plane loads, have been investigated in [3]. In particular, the turning circle qualities of a tanker like vessel have been analyzed by coupling the CFD solver with an hybrid propeller model based on the coupling between the Hough & Ordway model for the computation of thrust and torque, and the Ribner's theory for take into account for oblique flow effects. Numerical results demonstrated that propeller lateral force should be accounted for in order to correctly estimate the vessel's dynamic behavior.

As already introduced above, the numerical investigation carried out in this work is aimed to the analysis of simplified propeller models for their efficient and reliable inclusion into CFD solvers. In particular, the BEMT model, extended for the treatment of oblique flow effects [19]. In this preliminary investigation, the flow field generating around the model during straight and stabilized turning conditions are first computed by means of CFD solver. It has to be remarked that the main interest is in the evaluation of the nominal wake features in correspondence in both conditions. Therefore, propellers are not modeled. Once the nominal wake is evaluated, propeller hydrodynamic characteristic can be solved by means of the BEMT model.

MATHEMATICAL MODEL

The governing equations for the unsteady motion of an incompressible viscous fluid can be written in integral form as:

$$\begin{aligned} &\oint_{S(V)} \mathbf{U}\cdot\mathbf{n}\,\mathrm{d}S = 0 \\ &\frac{\partial}{\partial t}\int_V \mathbf{U}\,\mathrm{d}V + \oint_{S(V)} (F_C - F_D)\cdot\mathbf{n}\,\mathrm{d}S = 0 \end{aligned} \tag{1}$$

where V is a control volume, $S(V)$ its boundary and $\mathbf{n}$ the outward unit normal. In the general formulation, the equations are written in an inertial frame of reference, in order to take into account the possibility of grid motion. The equations are made non-dimensional with reference velocity U_∞, length L and the water density ρ. In equation (1), F_c and F_d represent inviscid (advection and pressure) and diffusive fluxes, respectively:

$$\begin{aligned} F_C &= p\mathbf{I} + (\mathbf{U}-\mathbf{V})\mathbf{U} \\ F_D &= \left(\frac{1}{Re} + \nu_t\right)\left(\nabla\mathbf{U} + \nabla\mathbf{U}^{\mathrm{T}}\right) \end{aligned} \tag{2}$$

In the previous equation, $p=P+z/Fr^2$ is the non-dimensional hydrodynamic pressure (i.e. the difference between the total non-dimensional pressure P and the hydrostatic pressure $-z/Fn^2$, $Fr=U_\infty/(gL)^{1/2}$ being the Froude number and g the acceleration of gravity parallel to the vertical axis z, positive upward), $\mathbf{V}$ is the local velocity of the control volume boundary, $Re=U_\infty L/\nu$ the Reynolds number, ν the kinematic viscosity, and ν_t the non-dimensional turbulent viscosity; in the present work, the turbulent viscosity was calculated by means of a proper turbulence model. In what follows, the Cartesian components of the velocity vector will be denoted by u_i with index notation or by u,v,w.

The problem is closed by enforcing appropriate conditions at physical and computational boundaries. On solid walls, the relative velocity is set to zero (whereas no condition on the pressure is required); at the (fictitious) inflow boundary, velocity is set to the undisturbed flow value, and pressure is extrapolated from inside; on the contrary, pressure is set to zero at the outflow, whereas velocity is extrapolated from inner points.

At the free surface, whose location is one of the unknowns of the problem, the dynamic boundary condition requires continuity of stresses across the surface; if the presence of the air is neglected, the dynamic boundary conditions read:

$$\begin{aligned} &p = \tau_{ij} n_i n_j + \frac{z}{Fr^2} + \frac{\kappa}{We^2} \\ &\tau_{ij} n_i t_j^1 = 0 \\ &\tau_{ij} n_i t_j^2 = 0 \end{aligned} \tag{3}$$

where τ_{ij} is the stress tensor, κ is the average curvature, $We=(\rho U_\infty^2 L/\sigma)^{1/2}$ is the Weber number (σ being the surface tension coefficient), whereas $\boldsymbol{n}$, $\boldsymbol{t}^1$ and $\boldsymbol{t}^2$ are the surface normal and two tangential unit vectors, respectively.
The actual position of the free surface $F(x,y,z,t)=0$ is computed from the kinematic condition:

$$\frac{\mathrm{D}F(x,y,z,t)}{\mathrm{D}t}=0 \tag{4}$$

Initial conditions have to be specified for the velocity field and for the free surface configuration:

$$\begin{aligned} u_i(x,y,z,0) &= \overline{u_i}(x,y,z) \qquad i=1,2,3 \\ F(x,y,z,0) &= \overline{F}(x,y,z) \end{aligned} \tag{5}$$

NUMERICAL METHODS

The numerical solution of the governing equations (1) is computed by means of the solver *χnavis*, which is a general purpose simulation code developed at CNR-INSEAN; the code yields the numerical solution of the unsteady Reynolds averaged Navier-Stokes (uRaNS) equations for unsteady high Reynolds number (turbulent) free surface flows around complex geometries (the interested reader is referred to [4][5][8][6] for details). The solver is based on a finite volume formulation with conservative variables co-located at cell center. The spatial discretization of the convective terms is done with a third order upwind based scheme, whereas the diffusive terms are discretized with second order centered scheme and the time integration is done by second order implicit scheme (three points backward). The solution at each time step is computed iteratively by a pseudo-time integration, that exploits an Euler implicit scheme with approximate factorization, local pseudo time step and multi-grid acceleration [13]. Although several turbulence models have been implemented in the code, in all the simulations reported the turbulent viscosity has been calculated by means of the one-equation model of Spalart and Allmaras [28].
Free surface effects are taken into account by a single phase level-set algorithm [5]. Complex geometries and multiple bodies in relative motion are handled by a dynamical overlapping grid approach [8]. High performance computing is achieved by an efficient shared and distributed memory parallelization [2].

PROPELLER MODELS

Theoretical basis of the two propeller models considered in present study are described in the next two paragraphs. The former one is based on the classical BEMT and is the most recognized one among the Naval Architecture Community; the latter one is similar to the previous one, whereas it accounts for the shedding of vorticity experienced by every propeller blade section when rotating in a non uniform flow field, namely the ship wake (both in straight ahead and manoeuvring conditions).

BEMT MODEL

In the Blade Element Momentum Theory the propeller is modeled as a series of two dimensional airfoils independent from each other; lift and drag acting on the generic section are easily evaluated if two dimensional hydrodynamic properties of the profile are known (in terms of C_L and C_D) on the whole range of incidence angles experienced by the section during a complete blade rotation. Usually, when the propeller is operating during a manoeuvre, sectional incidence angle can be large and stall (at model scale) and cavitation phenomena can arise, affecting the total load developed by the blade. If the 2D section hydrodynamic characteristics are defined for a relatively broad range of incidence angles, these effects can be partially taken into account and modeled. The traditional BEMT theory has been modified [19] in order to treat non symmetrical inflow condition; the effect of the transverse component of the flow modifies the tangential component of the flow, as it is schematically represented in Figure 8 (α_P in the formulas reported on the sketch is the same as β_{PROP} in the main text). In particular, it is evident that the inflow transverse component $V_{INF}sin\alpha_P sin\theta$ modifies the tangential velocity ωr due to propeller rotation (θ representing section's circumferential position and α_P the propeller incidence angle). When the inflow is variable over the disk, as is the case for a propeller working in the hull's wake, α_P has to be interpreted as a local incidence angle.

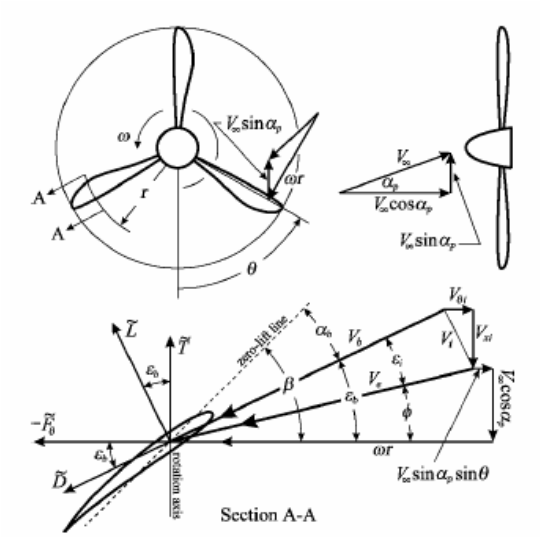

Figure 8: BEMT velocity definition [18]

As it is evidenced in the formulation presented below, the local incidence angle is implicitly taken into

account once the three components of the velocity field over the disk are provided. Sectional lift and drag are evaluated by means of the following formulas:

$$dL = 0.5\rho V^2{}_B c \frac{dC_L}{d\alpha}\alpha_{eff}$$
$$dD = 0.5\rho V^2{}_B c\left(C_{D0} + C_{D1}\alpha_{eff} + C_{D2}\alpha^2{}_{eff}\right) \quad (6)$$

where ρ is the fluid density, c is the profile chord and α_{eff} is the sectional angle of attack; hydrodynamic coefficient are pre calculated once the profile geometry is defined. V_B is the sectional velocity, resultant of longitudinal and transverse speed components, briefly defined below:

longitudinal component:

$$V_{axial} = u_{wake} + V_{ix} \quad (7)$$

circumferential component:

$$V_{axial} = \omega r + v_{wake}\cos(\theta) + w_{wake}\sin(\theta) + V_{i\tan} \quad (8)$$

where u_{wake}, v_{wake}, w_{wake} are the inflow components over the disk, r is the radial position of the section, θ is the circumferential position and V_{itan} and V_{ix} are the components of the propeller wake induced flow. These can be determined after the induced angle of attack ε_i is evaluated. To this aim the following relation based on Betz condition (relation between sectional circulation and transverse speed induced component) and Prandtl-Goldstein tip loss factor (accounting for propeller losses due to three dimensional effect), has to be solved:

$$\frac{Bc}{16r}\frac{dC_L}{d\alpha}(\phi_0 - \phi_\infty - \varepsilon_i) = \cos^{-1}\exp\left[-\frac{B(1-x)}{2\sin(\phi_{0T})}\right]\tan(\varepsilon_i)\sin(\phi_\infty + \varepsilon_i) \quad (9)$$

Due to its non linear character, this equation is solved by a common iterative technique in term of ε_i. In this relation, B is the number of propeller blades, Φ_0 is the geometrical pitch angle, Φ_{inf} is the incidence angle without considering induction effect and Φ_{0T} is the geometric pitch angle of the blade tip section. Once this equation is solved, the sectional flow is evaluated and the effective angle of attack can be determined:

$$\alpha_{eff} = \phi_0 - \phi_\infty - \varepsilon_i \quad (10)$$

In order to obtain sectional propeller thrust and torque, sectional lift and drag are first projected in the longitudinal and circumferential direction θ; total thrust and torque are calculated integrating sectional loads along the blade span and averaging in a propeller revolution; for the sake of brevity, only the propeller torque is derived:

$$dF_T = L\sin(\phi_\infty + \varepsilon_i) + D\cos(\phi_\infty + \varepsilon_i)$$
$$Q = \int_{R_{HUB}}^{R}\frac{B}{2\pi}\int_0^{2\pi} dF_T\sin(\theta)rdrd\theta \quad (10)$$

UNSTEADY BEMT MODEL

In order to account for the effects of the circumferential variations, and consequently, the unsteady nature of the inflow experienced by the propeller blade profiles during a complete revolution, the BEMT has been properly modified by means of 2D unsteady airfoil theory. The airfoil response due to a variable flow field (represented by both angle of attack and velocity magnitude) is modelled by beans of the Wagner theory, which is the time domain version of the Theodorsen's one [32] (which is developed in the frequency domain). The key aspect of present approach is that the airfoil inflow properties (angle of attack and speed) are properly modified due to (continuous) vortex shedding; this results in a modification of the sectional loads (lift and drag). In other words, the shedding of vorticity introduces a memory effect which causes a retardation in the airfoil response. From a physical point of view, unsteady motion modifies both potential (circulatory and inertial effects) and viscous (leading edge vortex/dynamic stall) related aspects.
The indicial method is based on the fundamental principle that the flow can be linearized with respect to the forcing function. The analytical solution is expressed as a time integral solved in a time (space) marching scheme which is second order accurate.
Let *s* denote a non dimensional time parameter given by:

$$s = \frac{2Vt}{c} \quad (11)$$

where V is the characteristic velocity, *t* is time and c is the propeller blade chord length. Physically, *s* denotes the stream wise distance in term of semi-chords. The time varying value of the sectional lift coefficient $C_L(t)$ can be expressed as a sum of two contributions, namely a circulatory effect and an added mass effect:

$$C_L(t) = C_{Lc}(t) + C_{Lnc}(t) \quad (12)$$

C_{LC} is a function of angle of attack in terms of the Duhamel integral as:

$$C_L(t) = C_{L\alpha}\left[\alpha(t_0) + \int_{s0}^{s}\frac{d\alpha}{dt}(\sigma)\phi(s-\sigma)d\sigma\right] = C_{L\alpha}\alpha_{eff}(t) \quad (13)$$

where ψ(s) is the indicial response to a unit step input and $C_{L\alpha}$ is the 2D lift coefficient slope; α_{eff} can be

interpreted as an effective angle of attack, with the integral term representing a retardation function modelling the shedding of vorticity. If the function inside the integral is assumed to be of the form:

$$\psi(s) = 1.0 - A_1 e^{-b_1 s} - A_2 e^{-b_2 s} \tag{14}$$

where the coefficients A_i and b_i are semi-empirical constant derived from oscillatory airfoil testing, therefore, functions of profile form and frequency of the motion.

The integral can be solved recursively, being the solution at the actual time *t* strictly dependent by the solution at the previous time step (instead of being affected by the all previous time history, as represented mathematically by (13)). Therefore, from the computational point of view, its computation is very efficient. Considering (14), (13) is rewritten:

$$\begin{aligned}
&\alpha_{eff}(s) = \alpha(s_0)\psi(s) + \int_{s0}^{s} \frac{d\alpha}{dt}(\sigma)\phi(s-\sigma)d\sigma = \\
&= \alpha(s_0)(1.0 - A_1 e^{-b_1 s} - A_2 e^{-b_2 s}) + \int_{s0}^{s} \frac{d\alpha}{dt}(\sigma)(1.0 - A_1 e \\
&- A_2 e^{-b_2(s-\sigma)})d\sigma \\
&= \alpha(s_0) - \alpha(s_0)A_1 e^{-b_1 s} - \alpha(s_0)A_2 e^{-b_2 s}\int_{s0}^{s} \frac{d\alpha}{dt}(\sigma)1.0 d\sigma \\
&- A_1 \int_{s0}^{s} \frac{d\alpha}{dt}(\sigma)e^{-b_1(s-\sigma)}d\sigma - A_2 \int_{s0}^{s} \frac{d\alpha}{dt}(\sigma)e^{-b_2(s-\sigma)}d\sigma =
\end{aligned} \tag{15}$$

Note that the time *t* has been substituted by the variable s, which can be viewed itself as a time. Neglecting the non integral terms (representing the initial value of angle of attack and the short term transient), (15) can be written as:

$$\begin{aligned}
&\alpha_{eff}(s) = \alpha(s) - X(s) - Y(s) \\
&X(s) = A_1 \int_{s0}^{s} \frac{d\alpha}{dt}(\sigma)e^{-b_1(s-\sigma)}d\sigma \\
&Y(s) = A_2 \int_{s0}^{s} \frac{d\alpha}{dt}(\sigma)e^{-b_2(s-\sigma)}d\sigma
\end{aligned} \tag{16}$$

Assuming a continuously sampled system with time step Δs, at time s+Δs it can be written:

$$\begin{aligned}
&X(s+\Delta s) = A_1 \int_{s0}^{s+\Delta s} \frac{d\alpha}{dt}(\sigma)e^{-b_1(s+\Delta s-\sigma)}d\sigma = \\
&A_1 e^{-b_1\Delta s}\int_{0}^{s} \frac{d\alpha}{dt}(\sigma)e^{-b_1(s-\sigma)}d\sigma + A_1 \int_{s}^{s+\Delta s} \frac{d\alpha}{dt}(\sigma)e^{-b_1(s+\Delta s-\sigma)}d\sigma = \\
&= X(s)e^{-b_1\Delta s} + A_1 \int_{s}^{s+\Delta s} \frac{d\alpha}{dt}(\sigma)e^{-b_1(s+\Delta s-\sigma)}d\sigma = X(s)e^{-b_1\Delta s} + I
\end{aligned} \tag{17}$$

It has to be observed that (17) is a one step recursive formula in terms of the previous value *X(s)* and a new increment, *I*, over the new period. Considering the evaluation of the increment *I*:

$$\begin{aligned}
&I = A_1 \int_{s}^{s+\Delta s} \frac{d\alpha}{dt}(\sigma)e^{-b_1(s+\Delta s-\sigma)}d\sigma = \\
&A_1 e^{-b_1(s+\Delta s)} \int_{s}^{s+\Delta s} \frac{d\alpha}{dt}(\sigma)e^{b_1\sigma}d\sigma = A_1 e^{-b_1(s+\Delta s)} \int_{s}^{s+\Delta s} \frac{d\alpha}{dt}(\sigma)\, f(\sigma) \\
&f(\sigma) = e^{b\sigma}
\end{aligned} \tag{18}$$

Then, solving numerically for the term ∂α/∂t:

$$\frac{d\alpha}{dt} = \frac{3\alpha(s+\Delta s) - 4\alpha(s) + \alpha(s-\Delta s)}{2\Delta s} \tag{19}$$

the remaining part of the increment can be solved exactly:

$$I = A_1 \frac{\Delta\alpha_{s+\Delta s}}{\Delta s}\frac{1-e^{-b_1\Delta s}}{b_1} \tag{20}$$

Analogous considerations can be made for *Y(s)*, giving:

$$\begin{aligned}
&X(s) = X(s-\Delta s)e^{-b_1\Delta s} + I_X \\
&Y(s) = Y(s-\Delta s)e^{-b_1\Delta s} + I_Y
\end{aligned} \tag{21}$$

From the above relations, it can be evidenced that *X(s)* and *Y(s)* contains all the time history information of the unsteady hydrodynamics.

The non circulatory component (namely the one accounting for added mass effects) is evaluated by Theodorsen theory which treats the airfoil as a flat plate accelerating in an ideal incompressible flow:

$$\begin{aligned}
&C_{Lnc} = \frac{\pi}{cV}\frac{d\alpha}{dt} \\
&\frac{d\alpha}{dt} = \frac{\alpha_{t-1} - \alpha_t}{\Delta t}
\end{aligned} \tag{22}$$

It has to be pointed out that, similarly to the circulatory lift component, the non circulatory one is also function of frequency of the motion. In present computations values suggested in [17] have been considered.

The sectional drag, is treated as a sum of two contribution, the one due to the mean flow reported in (6), plus an induced one related to trailing edge vortex shedding, strictly related to the lift:

$$\Delta C_{Di} = C_{LC}(\alpha - \alpha_{eff}) \tag{23}$$

where α is the nominal angle of attack and α_{eff} is defined in (16).

If the generic inflow components is separated into a mean and perturbation contribution, namely:

$$u_i(t) = \bar{u} + \Delta u(t) \tag{24}$$

then, the indicial theory is applied to the perturbation inflow, while the classical BEMT theory has been applied to the mean component.
It has to be noticed that present approach does not account for other physical aspects concerning the airfoil behaviour in an unsteady regime, such as: the pressure delay, i.e. the pressure distribution along the airfoil does not develop instantaneously, but is delayed due to retardation in the circulation development; and the leading edge vortex formation, or, alternatively, the dynamic stall. Numerical tests performed on the indicial model demonstrated that the former effect is negligible with respect to effective angle of attack delay. On the other hand, dynamic stall is a phenomenon that can be of fundamental importance in the analysis of propeller behaviour in off-design conditions or at high loadings [25][26], both at model scale, where cavitation are prevented but in depressurized atmosphere and stall phenomena manifests, or at full scale where cloud cavitation and bubble cavitation may assume the typical appearance of dynamic stall [14]. The extension of the indicial model to treat all the physical aspect of unsteady airfoil behaviour is straightforward, but due to the semi-empirical nature of the model, time constant need to be determined in advance and ad-hoc experiment should be performed to this task. Therefore, in order to analyse the basic flow characteristic, such aspects has not been included in this preliminary analysis.

GEOMETRY AND MESH

Model geometric characteristics are summarized in Table 1. In this investigation, a simplified geometry has been considered, consisting of the bare hull, bilge keels and centreline skeg. It can be observed that present approach is affordable because the strong vortical structures characterising the flow field of a manoeuvring vessel are generated in correspondence of the bilge keels and skeg.

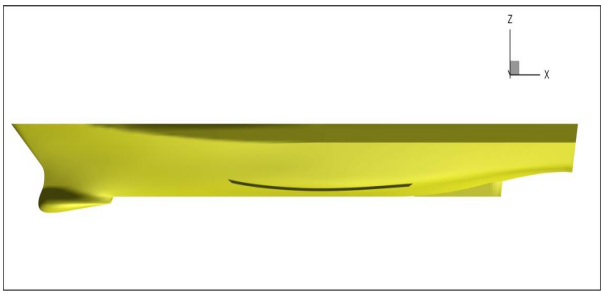

Figure 9: Simplified geometry considered

The computational grid used in the simulation was produced by the commercial mesh generator ICEM-CFD. It consists of 162 structured block with a total of about 9M grid cells; a detail of the discretization of the individual part of the vessel is summarized in Table 9. Grid distribution is such that the thickness of the first cell on the wall is always below 1 in terms of wall units at the highest F_N ($y^+=O(1)$, i.e. $\Delta/L_{pp}=O(20/Re)$, Δ being the thickness of the cell, L_{pp} the length between perpendiculars and *Re* Reynolds number).

NUMERICAL RESULTS

The main task of the numerical simulations is keep more insight into the nature of the flow field in correspondence of the propeller wake when the hull advances in a turning manoeuvre and analyse the propeller unbalancing and overloading phenomena by means of BEMT models described above. Last, but not least, the use of simplified propeller models is aimed to assess their potential coupling to general purpose CFD solver in order to reduce computational time in those cases where the details of the solution are not of crucial importance, rather, a reliable and physical estimation of propeller behaviour is of principal concern.

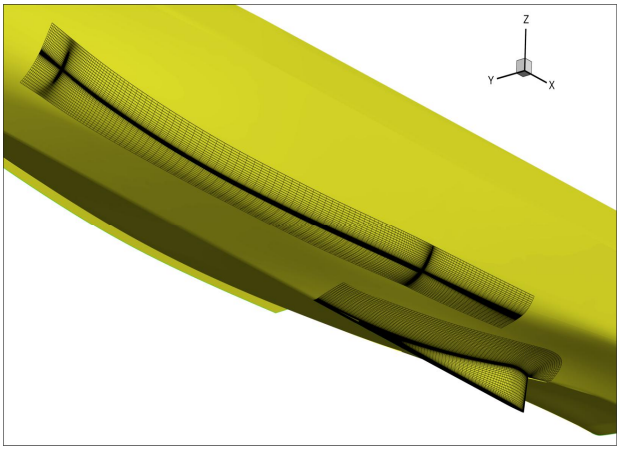

Figure 10: Mesh details over the bilge keel and skeg

Table 9 Overlapping blocks: details of the discretization.

Zone	N. of Blocks	N. of Volumes (x2)
Background	9	365,568
Free Surface	2	337920
Hull	48	2,353,152
Bilge Keels	18	1,148,928
Bilge Keels	18	1,148,928
TOTAL	87	4,767,232

To this purpose, the wake in correspondence of the propeller disks have been evaluated for the hull in the straight ahead condition and in a steady turn with the same attitude (drift angle) and rotational speed measured during the experiments. The hull has been maintained in the upright position, i.e. at zero roll angle; to justify this simplification, it has to highlight that, roll angles during the free model tests were relatively low in the stabilized phase (2° and 5° for the

lowest and highest $F_{N,}$ respectively). Computations presented in the following are relative to the lowest speed (F_N=0.267) only, because the unbalancing and overloading phenomena was found qualitatively similar for the two regimes. In this preliminary phase propeller RPM has been set equal to the value recorded during the experiment. In Table 10 numerical parameters are listed.

Table 10: Numerical parameters.

TEST	Fn	RPM	δ	β	R
1	0.267	7.5	0	/	/
2	0.196	7.5	35°	10°	2.2

The numerical solutions were computed by means of a Full Multi Grid-Full Approximation Scheme (FMG-FAS) [13], with four grid levels, each obtained from the next finer by removing every other grid points. In the FMG-FAS approximation procedure, the solution is computed on the coarsest grid level first; then it is approximated on the next finer grid and the solution is iterated by exploiting all the coarser grid levels available with a V-Cycle. The process is repeated up to the finest grid level. On each level, the iterative solution is carried on until the L_2-norm of the residuals drops of four orders of magnitude and the variation on the forces and moment is at most on the fourth digit. Test No.1 has been carried out on half-body in order to save computation time. Numerical computations relative to the turning have been carried out fixing the model at same kinematics attitude experienced during the free running tests; it has to be observed that the drift has not directly measure but derived indirectly from the heading and turning trajectory; the value of 10° is a reasonable value for a model of this type which is intrinsically stable due to the fine form geometry and presence of a relatively pronounced appendage area [9].

VERIFICATION

Verification, i.e. the evaluation of the order of convergence and the assessment of numerical uncertainty, has been carried out for the total resistance and, for the steady turn condition, also for the lateral force and the yaw moment. Results are summarized in Table 11. The values S_3, S_2 and S_1 are the non dimensional force or moment computed on the coarse, the medium and the fine grid, respectively; p_{RE} is the order of accuracy:

$$p_{RE} = \frac{\ln(\varepsilon_{32} / \varepsilon_{21})}{\ln(r)} \tag{25}$$

where $\epsilon_{21}=S_2-S_1$, $\epsilon_{32}=S_3-S_2$ and r is the grid refinement ratio ($r=2$ has been used in the current analysis). From the solution on the medium and the finest grid, the Richardson's Extrapolated error δ_{RE} can be computed:

$$\delta_{RE} = \frac{\varepsilon_{21}}{r^{p_{RE}} - 1} \tag{26}$$

The generalized Richardson Extrapolated solution S_{RE} can be then estimated as:

$$S_{RE} = S_1 - \delta_{RE} \tag{27}$$

When monotonic convergence is attained (i.e. $0<\epsilon_{21}/\epsilon_{32}<1$ both the order of convergence and the error can be computed. Several methods ([12][24][31][36][37]) can be used for the estimation of the numerical uncertainty; in the present work the factor of safety method [37] has been adopted. In this method, a measure for the distance from the asymptotic range is given by the ratio between the computed order of accuracy and the theoretical one, i.e. $P=p_{RE}/p_{th}$; when the solutions are in the asymptotic range P≈1, the actual order of convergence is equal to the theoretical value. This method has been proved superior to the correction factor method [31][36] since it overcomes the unreasonable small uncertainty estimation when the measured order of convergence is less than the theoretical value; moreover, it provides an overall *95\%* confidence level for the estimated uncertainty to bound the true error. According to the factor of safety method, the uncertainty can be computed as:

$$U_{FS} = \begin{cases} (2.45 - 0.85P)\left|\delta_{RE}\right| & \text{if} \quad 0 < P < 1 \\ (16.4P - 14.8P)\left|\delta_{RE}\right| & \text{if} \quad P > 1 \end{cases} \tag{28}$$

In Table 11, the estimated numerical uncertainties for the non-dimensional resistance, lateral force and yaw moment are reported, respectively; since negligible iterative uncertainty has been observed (well below *1%*, grid uncertainty can be considered as the only contribution to the numerical uncertainty). In case of monotonic divergence or oscillatory convergence, to estimate the extrapolated values, the classical Richardson extrapolation has been used (i.e. it has been assumed that the medium and the finest grid are in the asymptotic range, then the nominal order of convergence has been considered).

Table 11: Grid convergence study and numerical uncertainties for the non-dimensional lateral forces.

Fr	*Force*	10^3S_3	10^3S_2	10^3S_1	p_{RE}	10^3S_{RE}	U_{NS} [%S_{RE}]
0.267	***°X***	*0.52*	*0.396*	*0.404*	*Osc*	*0.406*	*-0.64%*
0.197	***X***	*0.55*	*0.515*	*0.594*	*Osc*	*0.602*	*-4.26%*
	Y	*1.06*	*1.135*	*1.181*	*0.37*	*1.24*	*11.66%*
	N	*-0.52*	*-0.55*	*-0.56*	*0.31*	*-5.695*	*12.08%*

Oscillatory behaviour has been found for the longitudinal force; on the other hand, the convergence

of lateral force and yaw moment is monotonic. Overall the uncertainty is rather poor, the grid quality analysis and refinement is on-going.

FLOW FIELD FEATURES DURING TURN

In Figure 11 the flow field around the stern region of the model is described in terms of axial velocity u, in order to appreciate the most important aspects affecting the propeller inflow during a steady turn; in particular, flow visualizations are described for transverse sections of the stern region (namely from x=-0.4 to x=0.1, where x is non dimensional in terms of model reference length). At x=-0.4 two vortices can be observed generated from the bilges; the vortex on the external side is mainly generated by the bilge keel, while on the leeward side interaction of the bilge keel and hull bilge vortex can be detected. Moreover, the boundary layer along the bottom of the hull is asymmetrical: in particular it is thicker on the internal side. At section x=-0.24 the bilge keel vortex on the external side moves towards the leeward side; similar dynamics can be observed for the combined bilge/bilge keel vortex on the leeside. At section x=-0.19 the windward vortex seems to detach moving towards the skeg; the skeg counter rotating vortex can be also evidenced. The intense vortex on the internal side is stable and moves far away from the hull. At section x=-0.14 a strong vortex interaction between the external bilge keel vortex and the skeg one can be evidenced; it seems that the phenomenon is likely due to the impact of the former one on the skeg.
In Figure 12, the hull wake in correspondence of the propellers' location can be observed; in particular, the axial flow field on the external propeller is not affected by the hull wake; on the other hand, the inflow on the internal one is more complicated because the disk is entirely covered by a strong vortex generating from the interaction of the bilge-skeg one with flow separating from the windward to the leeward side of the stern.
Finally, for the sake of completeness, in Figure 13 the free surface field during the turn is compared with the straight motion one. It is evident the wave pattern asymmetry induced by the curvilinear motion, in particular the Kelvin angle is reduced on the windward side and increased on the leeward side.

PROPELLERS OVERLOADING AND UNBALANCING ANALYSIS

Velocity field at the propeller location has been evaluated and passed off-line to the propeller solvers in order to evaluate thrust and torque. In order to carry out a preliminary validation of the propeller model, hydrodynamic characteristic (K_T and K_Q) in open water conditions have been calculated. As it can be evidenced in Figure 14, both thrust and torque coefficients are in good agreement with respect to experimental values, this being encouraging for the computation in the hull wake both in straight ahead and steady running motion.

x'=-0.4

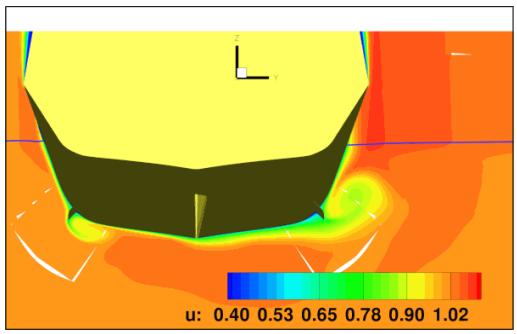

x'=-0.24

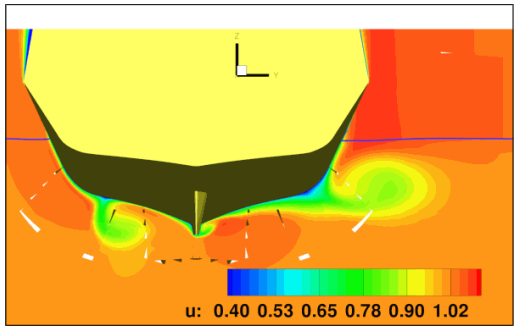

x'=-0.19

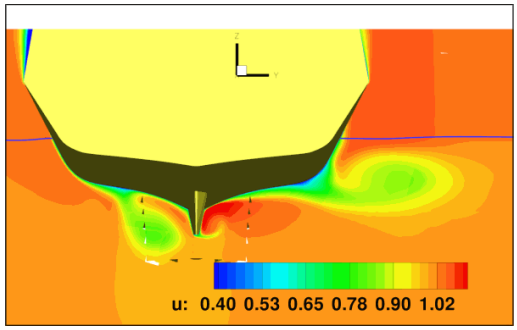

x'=-0.14

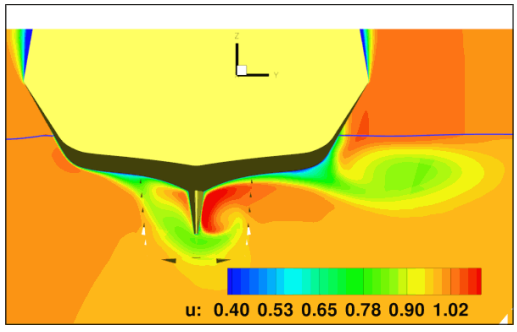

Figure 11: Axial velocity field

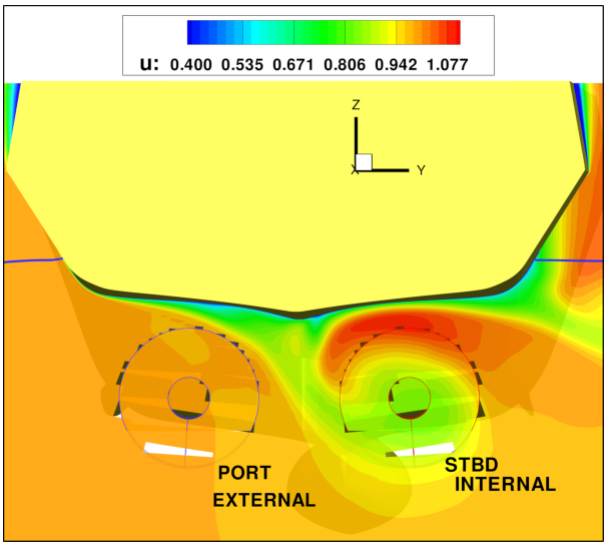

Figure 12: Axial velocity field close to propellers

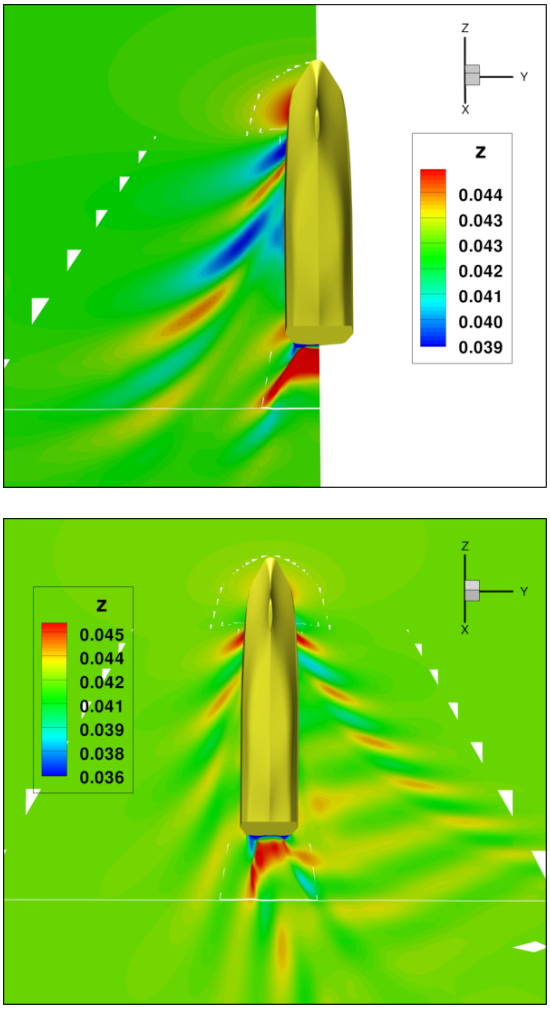

Figure 13: Free Surface field in approach and turning

In Figure 15 the model wake during straight ahead condition in correspondence of the propeller disk is represented in terms of axial velocity (u). Propeller loads evaluated by means of the two BEMT models for this condition are reported in the upper part of Table 12. It can be observed that discrepancies among the two numerical models in terms of resultant propeller loads are negligible. This can be further explained by examining Figure 16, where resultant load on a blade during a complete revolution are sketched. It can be observed that, despite the wave form, thrust/torque mean values reported in Table 12 are very similar, the indicial model experiences a delay in response as well as different maximum values.

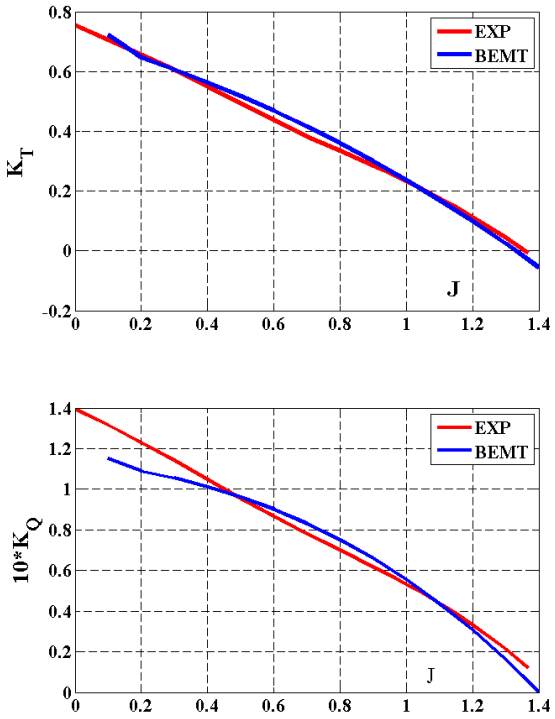

Figure 14: Open water propeller characteristic comparison

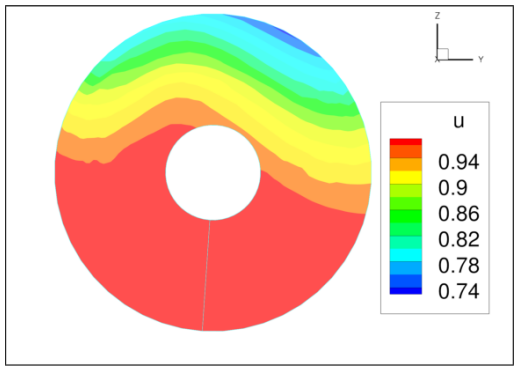

Figure 15: Hull wake longitudinal component

The more the propeller inflow is characterised by higher harmonic content, the more discrepancies between the two models (also with respect to mean value) may arise, as it will be shown in the following discussion. Hull wake in correspondence of the propeller planes is visualized in Figure 17 in terms of non dimensional longitudinal and horizontal (v) components because are the most affected one during the motion.

Table 12: Straight path propeller loads prediction

	BEMT	INDICIAL	EXP	ERR BEMT%	ERR INDICIAL %
K_T	0.218	0.2188	0.213 (0.6e-2)	2.34%	2,72%
K_Q	0.052	0.0523	0.044 (0.5e-2)	18%	18.86%

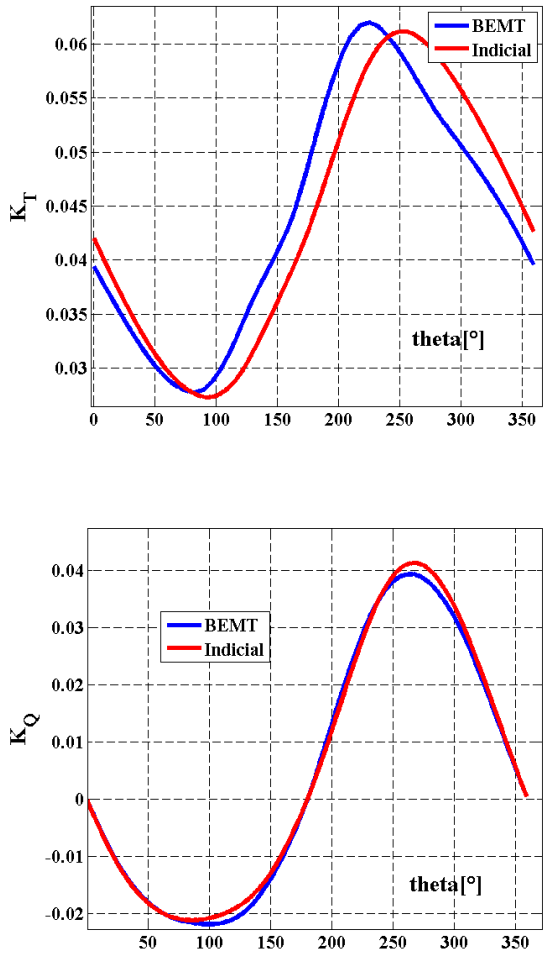

Figure 16: Blade Loads during a revolution

As it can be evidenced, the inflow on the external/windward propeller is not influenced by hull's wake with only a strong lateral (in-plane) velocity, clearly due to the combined yaw-drift motion. On the contrary, the wake on the leeward propeller is more complex because of the deflection of the boundary layer detaching from the hull and of the intense counter rotating vortex generated by the interaction of the bilge and the skeg ones. It can be observed that the longitudinal velocity is reduced up to 20% in the lower half of the disk; moreover, the lateral component is driven from the windward to the leeward side on the lower half of the disk and, from the leeward to the windward side on the upper half. This is mainly caused by the presence of the anticlockwise vortex. It has to be noticed that the wake feature over the propellers' disk is qualitatively similar to flow visualization at full [16] and model [1] scale.

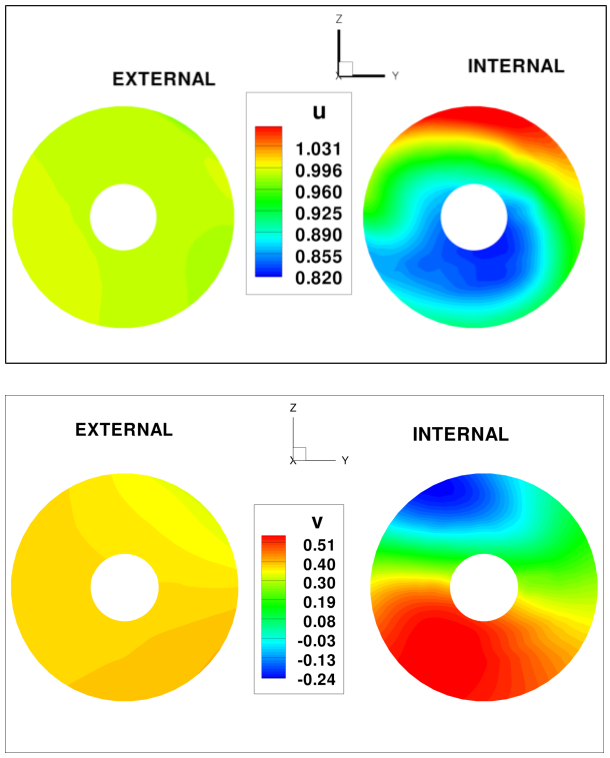

Figure 17: Propeller inflow during steady turn: u (up), v (down)

Numerical computations resulting from the two simplified propeller models are reported in Table 13, where thrust and torque are compared with the experimental measures. Moreover, in order to gain more insight into the phenomenon and to capture the key features, propeller loads have been evaluated considering the complete wake field and its longitudinal component only (in brackets). It can be observed that both approaches correctly predict the trend of the unbalancing (namely, the external shaft more loaded with respect to the internal one), as well as

the overloading phenomenon; moreover, thrust and torque absolute values are accurately predicted, the average error below 10%; in this case, the indicial model estimation is slightly better that the (steady) BEMT. On the other hand, calculated thrust and torque for the internal propeller are less accurate; in particular, the steady solver performs better than the unsteady one; in particular, discrepancies with respect to experiments for the former one are 15% and 25% regarding thrust and torque, respectively.

Table 13: Steady Turning propeller loads prediction

	INTERNAL		**EXTERNAL**	
	K_T	K_Q	K_T	K_Q
BEMT	0.27 (0.38)	0.058 (0.079)	0.35 (0.35)	0.0745 (0.0735)
INDICIAL	0.32 (0.39)	0.068 (0.08)	0.366 (0.349)	0.0746 (0.0735)
EXP	0.237 (0.011)	0.046 (0.004)	0.398 (0.017)	0.070 (0.006)
%ERR BEMT	15 (60)	25 (71)	-10 (-12.5)	6.57 (6)
%ERR INDICIAL	35 (64.55)	49 (74)	-8.06 (-12)	6.57 (5)

However, the unsteady solver fails in capturing correctly loads with 35% and 49% percentage error for thrust and torque. The poor accuracy for the indicial model can be related to the effective reduced frequency of the inflow: the indicial model, and, in particular, the semi empirical time constant modelling the airfoil unsteady behaviour, are valid for a prescribed frequency interval (typical of helicopter rotors, namely k=0.2 [25][26]), which may not be the case for a propeller working in a perturbed wake similar to the considered for the leeward side.

Moreover, it has to be emphasized that in such a cases only the longitudinal component u is considered, both the steady and indicial approaches fails in capturing the correct overloading trend (namely, the internal propeller is more loaded with respect to external one). In particular, the presence of the in-plane component does not affect the prediction on the external shaft, whereas the solution accuracy for the internal shaft is markedly reduced. The steady BEMT results can be considered quite promising for the purpose of its implementation in a CFD solver, because the physical phenomena involved in oblique flow condition, or alternatively, during off-design conditions, are captured. On the other hand, the indicial approach is attractive because it could be able to treat unsteady phenomena, at least if the coefficients representative of the impulsive response are validated for flows with frequencies contents typical of the hull wake. Moreover, it has to be pointed out that, the capabilities of the two models should be further verified for the fully appended hull.

In order to provide a global insight of the feature of hull wake close to the propeller disk, averaged values of the inflow have been computed; in particular, in Table 14 non dimensional value of wake lateral velocity and flow straightening coefficient on the internal and external propeller have been evaluated considering only the axial (u) and lateral (v) components. It can be observed that on the external shaft, v' is slightly higher with respect to the resulting one resulting from the motion, leading to a flow straightening coefficient (ratio of effective to the nominal lateral velocity due to the motion) higher than 1 (no flow straightening). This further confirms the velocity distribution reported in Figure 17, i.e. the presence of a strong lateral flow. On the other hand, the internal propeller, being in the hull wake, experience a flow straightening of about 30%. This analysis provide a further insight into possible ways to develop physical based models in simplified manoeuvring mathematical models, as proposed recently by [27][34].

Table 14: Average cross flow component on the propeller disk

	INTERNAL	**EXTERNAL**
v'_{PROP}	0.26	0.374
$v'_{DYNAMICS}$	0.372	
γ	0.69	1.02

A key aspect of the propeller behavior during off design conditions involves the generation of in plane forces on the propeller blades, which may affect the maneuvering response of the vehicle itself [1][3][9], and introducing further stress for the shafting equipment. In Figure 18 the lateral force component experienced by the internal and external propellers evaluated by means of the steady (continuous line) and unsteady BEMT models (dotted lines) are presented. For the sake of completeness, lateral forces in the approach phase is presented as well (green line). It can be observed that both models provide very similar result in the straight ahead and external cases, whereas different results are obtained for the internal propeller. This result points out that the wakes in the straight

ahead condition and in maneuver for the external propeller have a low harmonic content.
In the straight ahead condition, the lateral force is directed towards the hull symmetry plane; in the turning cases, both propellers exert a force from the wind to the lee side (e.g. provide a stabilizing effect), the internal one being the prevailing one. For the sake of completeness, the average value exerted by a single propeller blade over a complete shaft revolution are reported in Table 15.

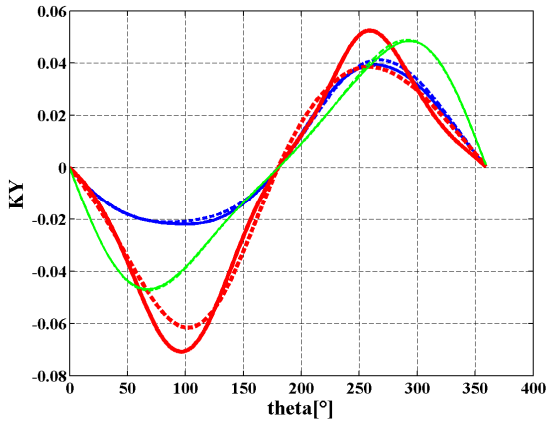

Figure 18: Blade Load lateral forces

Table 15: Average blade lateral force coefficient K_Y

	BEMT	INDICIAL
STRAIGHT	4.5e-3	5.03e-3
INTERNAL	5.4e-3	5.6e-3
EXTERNAL	4.8e-4	4.9e-4

CONCLUSIONS

In this works principal results of free running model tests carried out at different prime mover configurations have been presented and discussed. Measurements of propellers thrust and torque provide a detailed insight into off-design propulsion system, namely propellers overloading and unbalancing; this phenomenon may be of primary importance when dealing with non conventional propulsion system configuration, like cross-connect one, where the motion is transferred from the prime mover to the two shafts via a unique reduction gear. In this context, the automation control system strategy should be properly designed in order to prevent possible damages and, at the same time, not influence the vessel's operational tasks. In this experimental investigation it has been evidenced that when the propulsion system is set to deliver prescribed value of torque/power, maneuvering performance is not affected at all. Full scale trials are necessary in order to validate and confirm the procedure developed at model scale. Moreover, in order to gain a deeper insight into propeller off-design performances, numerical computations have been carried out. In this regard, it has to be pointed out that, propeller models which do not take into account for oblique flow effects, could lead to misleading results; on the contrary, the BEMT theory can be generalized to treat an arbitrary inflow variable in space (and in time) and oblique flow components. To this purpose, wake computed by the CFD solver has been passed (off-line) to two different BEMT based propeller models in order to compute thrust and torque on the internal and external sides. Qualitatively, both models correctly capture the overloading and the unbalancing between the two propellers. Thrust and torque on the external shaft are in good agreement with respect to the experiments, whereas, larger errors have been observed for the internal one. Comparing the two propeller models, large different results have been obtained for the internal shaft, the classical "steady" version being superior with respect to the indicial (unsteady) formulation. This analysis clearly showed that the key aspect of the unbalancing phenomena is related to oblique flow components over the propeller disk. This further confirms the demanding requirement of simplified propeller loads in modeling properly this effect. BEMT approaches can be a promising alternative; indeed, in this type of models, all the components of the velocity field are taken into account and therefore, it is suitable to capture the peculiar physical features experienced during off-design conditions.
Further experimental work is demanding to character the propeller behavior during off design conditions; in particular, in addition to thrust and torque, also in-plane loads, namely lateral and vertical forces, must be monitored. Moreover, BEMT model can be further corrected for deviation of the slipstream tube, which has been neglected in present computations. Regarding the unsteady (indicial) approach, the effects of the near wake trailed vorticity, which represent the wake region more affected by unsteadiness and provide a sort of 3D corrections, may be further considered. Last, but not least, this phenomenon certainly offer an ambitious test case for more sophisticated propeller models, like BEM and RANSE; in particular, the former one offer the better compromise between solution and resource demanding with respect to the latter one. In this perspective, the BEM model can be also used for keeping more insight into 3D effect and can certainly be valuable for validating new correction to BEMT representation. Finally, it has to be emphasized that the growing interests in propeller off design performance (driven also from novel propulsion device, like POD) may open new perspective in related research field; in particular, as stated in the main test, highly loaded propellers may be characterised by relevant viscous dynamic phenomena which are not well known among the naval community and can represent new trend regarding experimental activities.

AKNOWLEDGEMENTS

The work has been partially financed by the Italian Navy throughout the research project PROSSIMA and by the research project SUBMOTION II financially supported by the Italian and Norwegian navies, throughout the European Defence Agency.

REFERENCES

[1] Atsavapranee, P, Miller, R Dai, C, Klamo, J, Fry, D, 2010, ***"Steady-Turning Experiment and RANSE Simulations on a Surface Combatant Hull Form (Model #5617)"***, *28th ONR Symposium*, Pasadena.

[2] Broglia R., Di Mascio A., Amati, G., 2007. ***"A Parallel Unsteady RANS Code for the Numerical Simulations of Free Surface Flows"***, Proc. of 2nd International Conference on Marine Research and Transportation, Ischia, Naples, Italy.

[3] Broglia, R., Dubbioso, G., Di Mascio, A., 2011, ***"Prediction of Maneuvering Properties for a Tanker Model by Computational Fluid Dynamics***", Specialists Meeting on "Assessment of Stability and Control Prediction Methods for NATO Air and Sea Vehicles" (AVT-189) October 12-14, 2011, UK.

[4] Di Mascio A., Broglia R. Favini, B., 2001, ***"A second order Godunov-type scheme for naval hydrodynamics, in: Godunov Methods: Theory and Applications"***, Kluwer Academic/Plenum Publishers. pp. 253–261.

[5] Di Mascio A., Broglia R. and Muscari R., 2007, ***"On the application of the single-phase level set method to naval hydrodynamic flows"***, Computers & Fluids 36, 868–886.

[6] Di Mascio, A., Broglia, R., and Muscari, R. (2009). ***"Prediction of hydrodynamic coefficients of ship hulls by high-order Godunov-type methods"***. J. Marine Sci. Tech., Vol. 14, pag. 19-29.

[7] Di Mascio A., Dubbioso G., Notaro C., Viviani M., 2011, ***"Investigation of twin screw naval ships manoeuvring behaviour"***, Journal of Ship Research, accepted for publication.

[8] Di Mascio, A., Muscari, R., and Broglia, R. (2006). ***"An Overlapping Grids Approach for Moving Bodies Problems"***. 16th ISOPE, San Francisco, California (USA).

[9] Dubbioso, G., "***Manoeuvrability Behaviour of twin screw vessels***", PhD Thesis, Genova University, April 2011.

[10] Dubbioso, G, Mauro, S., Viviani, M., "***Off-Design Propulsion Power Plant Investigations by Means of Free Running Manoeuvring Ship Model Test and Simulation Techniques"*** Proceedings of the Twenty-first (2011) International Offshore and Polar Engineering Conference, p.943-950, Maui, Hawaii, USA, June 19-24, 2011, ISBN 978-1-880653-96-8 (Set); ISSN 1098-6189 (Set)

[11] Durante D., Broglia R., Muscari R. and Di Mascio A., "***Numerical simulations of a turning circle maneuver or a fully appended hull"***, 28th Symposium on Naval Hydrodynamics, Pasadena (Ca), 12-17 September 2010.

[12] Eca, L., Hoekstra, M., 2007, **"Discretization Uncertainty Estimation based on a Least Squares version of the Grid Convergence Index"**, 2nd Workshop on CFD Uncertainty Analysis, Lisbon, Portugal.

[13] Favini, B., Broglia, R., and Di Mascio, A. (1996). ***"Multigrid Acceleration of Second Order ENO Schemes from Low Subsonic to High Supersonic Flows"***. Int. J. Num. Meth. Fluids, vol. 23, pag. 589-606.

[14] Hoekstra, M., "**Exploratory RANS simulations of partial cavitation and its dynamics**"; MARINE 2011, Lisbon

[15] Hough G.R. and Ordway D.E., ***"The generalized actuator disk"***, Developments in Theoretical and Applied Mechanics, 2:, pag. 317-336, 1965.

[16] Kuiper, G, Grimm, M., McNeice, B., Noble, D., Krikke, M., 2002, ***"Propeller Inflow at Full Scale during a manoeuvre"***, *24th ONR Symposium*, Fukukoa

[17] Leishmann, G., 2006, "**Priciples of Helicopter Aerodynamics**", J. Wiley

[18] Lewis, E.W., 1988, "***Principles of Naval Architecture"***, SNAME

[19] Phillips, W.F., Anderson, E.A., Kelly, Q.J., 2003, ***"Predicting the Contribution of Running Propellers to Aircraft Stability Derivatives"***, Journal of Aircraft, Vol.40, No.6

[20] Phillips, A.B., Turnock, S.R. and Furlong, M.E., 2009, ***"Evaluation of manoeuvring coefficients of a self-propelled ship using a blade element momentum propeller model coupled to a Reynolds averaged Navier Stokes flow solver"*** *Ocean Engineering*, 36, 1217-1225.

[21] Phillips, A.B., Turnock, S.R. and Furlong, M., 2008, ***"Comparisons of CFD simulations and in-service data for the self propelled performance of an Autonomous Underwater Vehicle***", *27th Symposium of Naval Hydrodynamics, Seoul, Korea, 05 - 10 Oct 2008.* Seoul, Korea, Office of Naval Research

[22] Phillips A.B., Turnock S.R., Furlong M.E., ***"Accurate Capture of Rudder-Propeller Interactions using a coupled Blade Element–RANS Approach"***, 12th Numerical Towing Tank Conference, 2009.

[23] Ribner, H.S, ***"Propeller in yaw"***, NACA TECHNICAL REPORT 3L09, 1943.

[24] Roache, P.J., 1997, "Quantification of uncertainty in computational fluid dynamics" Ann. Rev. Fluid Mech. 29, 123–160.

[25] Shen, Y., Fuhs, D., "**Blade section lift coefficients for propellers at extreme off design conditions",** , 1997, CRDKNSWC/HD-1205-02 Report, Charderock Division

[26] Shen, Y., Fuhs, D., 1999, "**Dynamic effect on propeller blade section lift, drag, and pitching moment coefficients",** CRDKNSWC/HD-1205-02 Report, Charderock Division

[27] Shulten, P.J.M., 2005, "***The interaction between diesel engines, ship and propellers during manoeuvring"***, PhD-thesis, Delft University of Technology, 2005

[28] Spalart P.R. and Allmaras S.R., ***"A One-Equation Turbulence Model for Aerodynamic Flows"***, La Recherche Aerospatiale 1 (1994) 5-21.

[29] Stern, F. and Agdrup, K. (2008). Proceedings of Workshop on Verification and Validation of Ship Manoeuvering Simulation Methods, Copenhagen, Denmark.

[30] Stern F., Agdrup K., Kim S.Y., Cura-Hochbaum A., Rhee K.P., Quadvlieg F., Perdon P., Hino T., Broglia R., Gorski J., ***"Experience from SIMMAN 2008 - The first workshop on verification and validation of ship manoeuvring simulation methods"***, Journal of Ship Research, Vol. 55, No. 2, June 2011, pp. 135–147.

[31] Stern, F., Wilson, R.V., Coleman, H.W., and Paterson, E. (2001), **"Comprehensive Approach to Verification and Validation of CFD Simulations-Part 1: Methodology and Procedures"**. J. Fluid Eng., 123:793-802.

[32] Theodorsen, T., 1949, **"General Theory of aerodynamic instability and the mechanism of flutter"**, NACA REPORT No. 496

[33] Tian, Y., Kinnas S.A., 2011, "**Modelling of leading edge vortex and its effect on propeller performance",** 2nd International Symposium on Marine Propellers, Hamburg

[34] Viviani, M, Altosole, M., Cerruti, M, Menna, A., Dubbioso, G., (2008) ***"Marine Propulsion System Dynamics During Ship Manoeuvres"***, 6th International Conference On High-Performance Marine Vehicles (Hiper 2008) , 18/19/09/2008 – Naples, ISBN: 8890117494, p.81-93

[35] Viviani, M., Podenzana Bonvino, C., Mauro, S., Cerruti, M., Guadalupi, D., Menna, A., **"Analysis of Asymmetrical Shaft Power Increase Durino Tight Manoeuvres"**, 9th International Conference on Fast Sea Transportation (FAST 2007), Shangai, China, September 2007

[36] Wilson, R.V., Stern, F., Coleman, H.W., and Paterson, E., 2001, **"Comprehensive Approach to Verification and Validation of CFD Simulations--Part 2: Application for RANS Simulation of a Cargo/Container Ship",** J. Fluid Eng., Vol. 123, pag. 803-810.

[37] Xing, T., Stern, F., 2010, **"Factors of safety for Richardson Extrapolation",** J. Fluid Eng., Vol. 132, 061403-1.